RSC Advances

PAPER

View Article Online
View Journal | View Issue

Cite this: *RSC Adv.*, 2024, **14**, 31217

Direct patterning of liquid materials on flat and curved substrates using flexible molds with through-hole and post arrays†

Youngchul Chae,[a] Juyeol Bae [b] and Taesung Kim *[ac]

Liquids undergo continuous deformation in the presence of external shear stresses; however, they are pinned between structures owing to their viscosity. Therefore, reshaping the liquids using their intrinsic material properties and structural interfaces is possible. In this study, we used the template-guided forming (TGF) method to reshape and produce oil patterns on flat and curved substrates. To produce oil patterns, we developed two oil patterning methods: direct heating-based oil patterning (DHOP) and solvent evaporation-based oil patterning (SEOP), which were characterized using various oils and solvents. To overcome the limitation of relying solely on liquid patterning that undergoes complete evaporation, we successfully fabricated liquid films using oil and nonpolar organic solvents that exhibit long-term stability. Therefore, achieving durability and control over the film thickness using nonpolar organic solvents has great potential for future applications in microfluidics. Furthermore, we demonstrated that the SEOP method in conjunction with TGF can produce various and unconventional patterns of an organic photoresist (SU-8), which cannot be produced through standard photolithography. Hence, we conclude that the proposed TFG-based oil pattering methods could be highly useful for producing unconventional and unprecedented patterns on flat and curved substrates for various applications, including microelectronics, optics, filtration and separation, biomedical engineering, and nanotechnology.

Received 19th July 2024
Accepted 25th September 2024

DOI: 10.1039/d4ra05252h

rsc.li/rsc-advances

Introduction

Liquids undergo deformation when an external force is applied. Efforts have been made to engineer these liquids into desired shapes for application in the field of microfluidics.[1,2] Recent advancements in micro/nanofabrication technology have substantially enriched the research on applying patterning techniques using interfaces to control the shape and behavior of liquids.[3–6] Furthermore, several techniques have been developed to enhance the resolution while being inexpensive by combining the advantages of soft lithography, a bottom-up approach, and microfluidic manipulation.[7,8] Recently, Bae *et al.*[9] developed a membrane-assisted micro/nanofluidic liquid-mediated patterning technology. The liquid patterning technique using a microfluidic device allows the evaporation of a liquid to occur naturally through the microholes in the device. This facilitates the fixation of the evaporating liquid onto the microposts, forming a two-dimensional film.[10] Patterning has been primarily performed using water or organic materials alone; however, some studies have used water and oil simultaneously for patterning.[11–14] When patterning is performed using only one material, the range of application is limited. To overcome this limitation, studies are being conducted using the new properties of emulsions, which are a mixture of two liquids. Previously, an oil/water emulsion was used to fabricate porous membranes with omniphobic surfaces that exhibited liquid repellency.[15] However, oil and water produce low-precision patterns owing to their intrinsic immiscibility. Nevertheless, Wan *et al.*[16] demonstrated a precise surface patterning technique using hydrophilic/hydrophobic interactions for two immiscible phases on an organohydrogel surface with different wettability regions. Moreover, it is possible to achieve synchronous surface patterning of immiscible fluid pairs of air, water, and oils but these patterns are dynamic and can only persist for a short time. Recently, the formation and stabilization of oil-based foam liquids have been reported.[17] However, the stability and durability of oil film remain a great challenge, which is addressed in the present study.

Micro/nanofluidic liquid-mediated patterning techniques used liquid–air interfaces and can be further categorized into two groups: techniques without templates[18] and those with microstructures[19,20] or nanostructured templates.[21,22] Numerous pioneering studies utilizing structured templates, such as ice

[a]*Department of Mechanical Engineering, Ulsan National Institute of Science and Technology (UNIST), 50 UNIST-gil, Ulsan 44919, Republic of Korea. E-mail: tskim@unist.ac.kr; Fax: +82-52-217-2409; Tel: +82-52-217-2313*

[b]*School of Mechanical Engineering, Chonnam National University, 77 Yongbong-ro, Buk-gu, Gwangju 61186, Republic of Korea*

[c]*Department of Biomedical Engineering, Ulsan National Institute of Science and Technology (UNIST), 50 UNIST-gil, Ulsan 44919, Republic of Korea*

† Electronic supplementary information (ESI) available. See DOI: https://doi.org/10.1039/d4ra05252h

crystals,[23] leaf skeletons,[24] and nanoimprinted stamps, have demonstrated the widespread success of this approach in fabricating high-performance patterned devices. However, the preparation of templates requires expensive micro/nanofabrication processes and presents ongoing challenges. To address this issue, in this study, we utilized the template-guided foaming (TGF) technique, a one-step printing method that facilitates patterning on a three-dimensional (3D) curved substrate with initial curvatures.[9] The TGF mold featured a monolithic design comprising through-hole and post arrays and was prepared by layering a film of off-stoichiometry thiol–ene polymer resin (OSTEMER) on a polydimethylsiloxane (PDMS) frame with a through-hole and micropost array.[25] OSTEMER possesses favorable material strength (Young's modulus of 1000 MPa)[26] compared with PDMS and exhibits chemical resistance, thereby providing flexibility and mechanical strength to the mold. Moreover, the chemical resistance of OSTEMER eliminates restrictions on the use of aqueous nanomaterials, including perovskites, photoresists, and organic semiconductors.[26] The TGF method allows the use of aqueous nanomaterials such as perovskites, photoresists, and organic semiconductors.[27] For instance, the TGF method was utilized to fabricate flexible transparent conducting electrodes (FTCEs) on curved substrates using silver nanowires and conductive polymers in our previous study.[25] Furthermore, we have previously characterized the performance of FTCEs for their electrical and mechanical properties. In the present study, we employed the TGF method for patterning flexible and highly durable liquid films and characterized them according to the temperature conditions and solvent type. To overcome the limitations of patterning electrodes using only a water-containing dispersion, liquid films were synthesized using oil instead of water.[28] Furthermore, to the best of our knowledge, the performance characterization of oil patterns on flat and curved substrates has not been investigated.

Hence, in this study, we developed two oil-patterning methods – direct heating-based oil patterning (DHOP) and solvent evaporation-based oil patterning (SEOP) – that enabled the production of various oil patterns on flat and curved substrates. The TGF method allowed us to manipulate the patterns and shapes of oils on the substrate, followed by fine patterning. The DHOP method involves the direct evaporation of oils through heat application, whereas the SEOP method involves evaporating the solvents by dissolving the oils. We characterized the experimental conditions of DHOP and SEOP methods and analyzed the resulting thickness and durability of oil films formed by the hole and post arrays. We applied the SEOP method not only to form oil patterns on a transparent, flexible, and curved substrate but also to fabricate unconventional patterns of an organic photoresist that cannot be produced by conventional standard photolithography, which is followed by the solidification of the patterned photoresist. It is anticipated that the patterning methods in conjunction with the liquid materials used will provide various patterned liquid films by adjusting the air/oil interfaces using oil, organic solvents, and heat.

Materials and methods

Reagents and materials

PDMS (Sylgard 184, Dow Corning), OSTEMER (322 Crystal Clear, Mercene Labs), and poly(vinyl alcohol) (PVA; molecular weight = 89 000–98 000, ≥99% hydrolyzed; 341584, Sigma Aldrich) were utilized for the fabrication of through-hole and post arrays. For the surface modification of through-hole and post arrays, chlorotrimethylsilane (TMSCI; 386529, Sigma-Aldrich) and trichloro(1*H*,1*H*,2*H*,2*H*-perfluorooctyl)silane (PFOCTS; 448931, Sigma-Aldrich) were used. To fabricate liquid films within the through-hole and post arrays, hexadecane (anhydrous, ≥99%; 296317, Sigma-Aldrich), hexane (anhydrous, 95%; 296090, Sigma-Aldrich), octane (anhydrous, ≥99%; 296988, Sigma-Aldrich), and toluene (anhydrous, 99.8%; 244511, Sigma-Aldrich) were used. Furthermore, CdSe/ZnS quantum dots (powder, hydrophobic, 630 ± 5 nm: λ, Plasma-Chem) were incorporated into the nonpolar organic solvents to investigate the structure of the liquid. The SU-8 series used in the experiment, SU-8 2005 and SU-8 2010, were obtained from Kayaku Advanced Materials, MA 01581 USA, and the AZ series, AZ GXR 601, AZ GXR 601, AZ P4330, AZ 9260, AZ 5214, and AZ nLOF 2035, were obtained from AZ Electronic Materials.

Fabrication of molds with through-hole and post arrays

We followed a previously reported method for fabricating molds with through-holes and post arrays.[29] We used a standard photolithography process (refer to Fig. S1†) to fabricate the SU-8 master mold required for microfluidic devices. Initially, a negative photoresist (SU-8 2050, Kayaku Advanced Materials) was spin-coated onto a silicon wafer to a height of 50 μm and soft-baked. After exposure to ultraviolet (UV) light using a photomask and a mask aligner (MA6, SussMicroTec), a post-exposure baking process was performed. To ensure better adhesion between the wafer and the photoresist in the second layer, HMDS (HMDS; 440191, Sigma-Aldrich) was spin-coated and soft-baked. The second layer was spin-coated to a height of 25 μm using a different photoresist (SU-8 2025, Kayaku Advanced Materials), followed by soft baking. UV light exposure using a second photomask and mask aligner and a post-exposure bake were performed. The unexposed photoresist was removed by immersing the wafer in the SU-8 developer (Kayaku Advanced Materials). Finally, the wafer was subjected to a hard baking process to complete the photolithography process.

To fabricate the PDMS mold, the SU-8 master mold surface was chemically functionalized to render it hydrophobic using PFOCTS. For the soft lithography process, the PDMS base and a curing agent were mixed in a 10 : 1 ratio, and this mixture was degassed under vacuum for 30 min. The PDMS mixture was poured into the SU-8 master mold and cured in an oven at 65 °C for 3 h. Subsequently, the resulting PDMS mold was detached from the SU-8 master mold, and its surface was chemically functionalized using TMSCI.

To fabricate the OSTEMER membrane with through-hole and post arrays, the replicated PDMS mold was detached from

the SU-8 master mold and chemically functionalized to have a hydrophobic surface using TMSCI. A water-soluble sacrificial layer was produced by spin-coating PVA onto glass, and the PDMS mold was placed on top of it. Negative pressure was generated in the microchannel between the PDMS mold and the water-soluble sacrificial PVA layer on the glass by degassing the air within the PDMS mold under vacuum. OSTEMER resin was injected through the inlet hole, and the PDMS mold and water-soluble sacrificial PVA layer remained in contact through van der Waals interactions while the OSTEMER resin was loaded. Once the loading was complete, the OSTEMER resin was solidified under UV light at a wavelength of 365 nm for 5 min. The PDMS mold was then detached and reused. The solidification of the OSTEMER resin was completed by heating it in the oven at 90 °C for 3 h. Finally, the sacrificial PVA layer was dissolved in deionized water to detach the through-hole and post-array membranes from the glass.

Experimental setup

The liquid patterning process was analyzed using an inverted fluorescence microscope (IX71, Olympus Corp.) equipped with a charge-coupled device camera (Clara Interline CCD, Andor Technology, Ltd.). The microscope was automated using a motorized stage (BioPrecision2), motorized focus controller (99A400), and controller system (MAC 6000) provided by Ludl Electronic Products. A customized humidity/temperature-controlled system was used to ensure controlled atmospheric conditions. This system included solenoid valves (S10MM-20-24-2, Pneumadyne Inc.), a humidity/temperature sensor (SHT15, Sensirion), and a microcontroller board (Arduino Uno R3, Arduino CC), which were programmed using LabVIEW software (National Instruments Corp.). During the microscopic experiments, image capture was facilitated using imaging software (MetaMorph v7.8.10.0, Molecular Devices). Quantitative analysis of the fluorescence intensities in the captured images was conducted using ImageJ software (National Institutes of Health, Bethesda). The resulting normalized fluorescence intensities were plotted using OriginPro 2020 software (OriginLab Corp.). For high-resolution imaging of the through-hole and post arrays, a field-emission scanning electron microscope (S-4800, Hitachi) was employed with a 2 nm platinum layer sputtered on the surface. The shape of the liquid films within the membrane was observed using a confocal microscope (LSM 780 NLO, Carl Zeiss), and images were captured and analyzed using ZEN software (Carl Zeiss).

Results and discussion

Working principle generating oil films/patterns

We used the TGF method to achieve the one-step printing of liquid-mediated nanomaterials on flat substrates,[27,30,31] which enabled us to create oil-based patterning on the substrate. We designed and fabricated the interlayer membrane required for the TGF method, as shown in Fig. 1a. The membrane heights of the through-hole and post of the device were 50 μm and 25 μm, respectively. The diameter of the through-hole and post were 60 μm and 30 μm, respectively, and the spacing between the post walls was 40 μm. Fig. 1b illustrates the process of liquid-film patterning using a mixture of oil (hexadecane) and an organic solvent (hexane, octane, and toluene). A mixture of oil and nonpolar organic solvents was pipetted onto the OSTEMER membrane through a hole, allowing the drops to spread into the membrane and fill all empty spaces. As a result, the liquid area becomes thinner owing to air pressure. The presence of a through-hole in the microfluidic device creates an open system that promotes the natural evaporation of the liquid. This eliminates the occurrence of the Ostwald ripening phenomenon, in which larger air bubbles absorb smaller air bubbles.[32] The evaporating liquid was then fixed to the posts, and the liquid films were patterned.

To understand the shape of the liquid films, images were captured using a confocal microscope after injecting fluorescent quantum dots into an oil mixture (Fig. 1c). The mixture was prepared by mixing octane with hexadecane at a ratio of 9 : 1 and then injecting it into the OSTEMER membrane. The 3D shape of the oil film was visualized using confocal microscopy. The middle part of the liquid film appeared concave inward, providing insights into the shape of the oil films, as illustrated in Fig. 1b (middle). Initially, discretized circular oil–air interfaces were formed beneath the individual holes (depicted as bold black lines in Fig. 1b, bottom). These cylindrical interfaces uniformly expanded laterally in a concentric manner, encircling the holes and facing each other, and transformed into thin liquid films with lamellar structures.[33] Each post served as an anchor for six of these films. As evaporation progressed, the thickness of the films continued to decrease. The presence of oil ensured that the thin liquid films did not rupture by maintaining a balance between the Laplace and disjoining pressures.[34]

Using this working principle, oil films/patterns were generated on both flat and flexible substrates. The methods employed can be categorized into two cases: DHOP and SEOP. In the DHOP method, hexadecane was injected into the OSTEMER membrane. Subsequently, the membrane was heated on a plate to facilitate the evaporation of hexadecane, resulting in the formation of an oil film. Heat was gradually applied to the membrane once it was filled with hexadecane, allowing the progressive evaporation of the oil. This process led to the creation of oil films with oil/air interfaces as the air expanded through the through-holes and filled the spaces between the posts. By contrast, the SEOP method involved mixing an organic solvent with the desired target oil. The oil–solvent mixture was injected into the OSTEMER membrane, and only the organic solvent experienced gradual evaporation overtime, whereas the oil remained. This selective evaporation of the solvent led to the formation of oil films.

Characterization of oil film thickness

We characterized the ability to control the thickness of oil films fabricated using the DHOP and SEOP methods. First, we employed the DHOP method, in which the thickness of the oil films was controlled by adjusting the temperature and duration

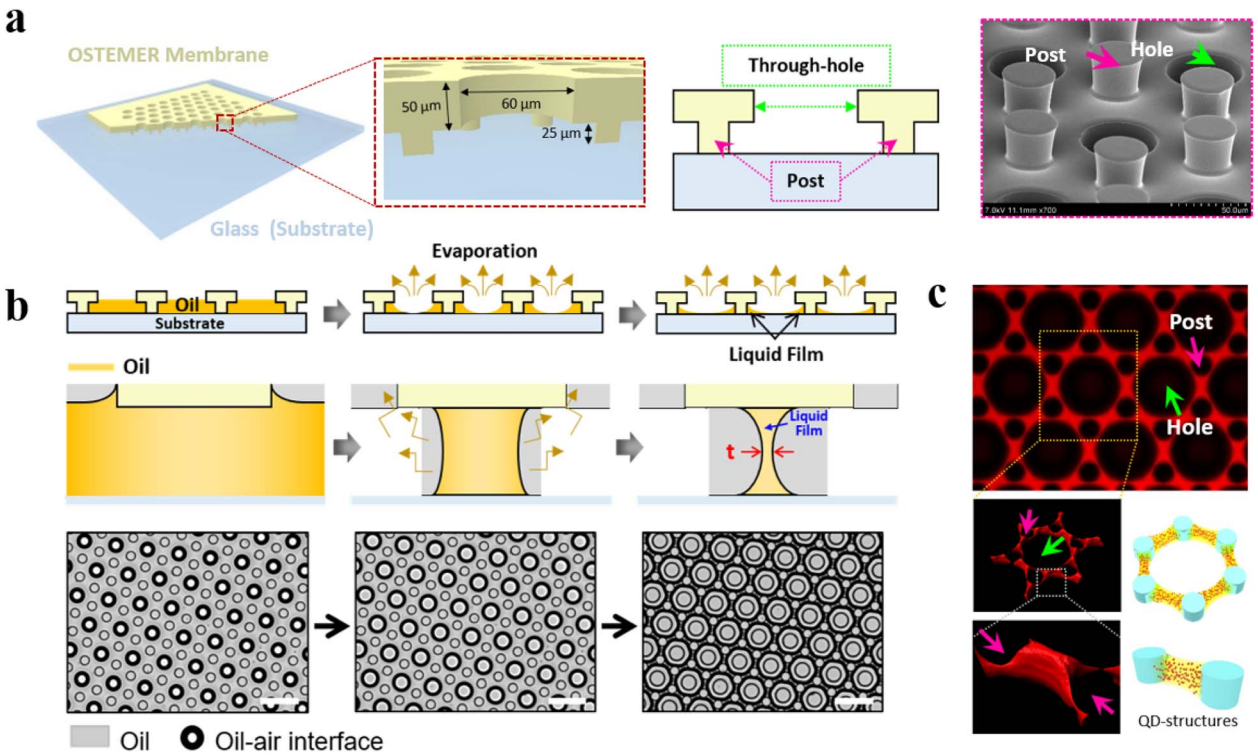

Fig. 1 Schematic of the working principle and formation process of oil patterns. (a) Structures of the OSTOMER membrane with through-holes and posts (left). The SEM image shows a microfabricated OSTEMER membrane (far right). (b) Fabrication process of the TGF-based liquid film in which through-holes and posts play a key role (top row, cross-sectional side view). As nonpolar organic solvents in the mixture of oil and solvents evaporate, the remaining oil forms liquid films (middle row, cross-sectional side view). The red "*t*" represents the thickness of the liquid film (middle row, side view). Microscopic images of the liquid film formation process (bottom row, top view). The black circles and thick lines represent air–oil interfaces, which increase as the solvent evaporates with time. Scale bars are 120 μm. (c) Fluorescent image (top) and confocal images (bottom left). Quantum dots (CdSe/Zns) are dissolved in a mixture of octane and hexadecane at a ratio of 9 : 1. 3D schematic images illustrating the mixture of octane oil and quantum dots (bottom and right). Purple and light green arrows indicate posts and through-holes, respectively.

of the heat applied to the OSTEMER membrane (Fig. 2). The change in the thickness of the oil films was measured by varying four distinct temperatures applied to the membrane (70, 80, 100, and 130 °C; Fig. 2b). In addition, after the heating temperature was fixed at 100 °C, different heating durations (10, 11, 12, and 13 min) were tested, which resulted in four different film thicknesses (Fig. 2d). (Fig. 2a depicts the change in the thickness of the oil film over time at 70 °C when applied to the membrane. The oil evaporates through the hole, and the circular shape of the oil–air interface rearranged in agreement with Plateau's law, thus leading to a decrease in the film thickness as the time progressed. Fig. 2c shows the images of the oil film pattern when the oil film was heated at 100 °C for 10 min, allowing it to evaporate, and a variation in the film thickness was observed. The circular pattern recedes as the air pushed the oil, resulting in a decrease in the film thickness over time. The stability of the films was assessed by incubating them at room temperature for an extended period. Liquid films with a thickness of 3–4 μm were maintained until day 8, whereas those with thicknesses of 2 μm were maintained until day 7. Liquid films with thicknesses below 1 μm remained stable until day 3. Owing to the hydrophobic nature of both the membrane and the oil, injection of oil was possible. Although hexadecane oil has a high boiling point (286.9 °C), evaporation occurs when the temperature is gradually applied. The oil evaporated through the holes in the membrane and consequently decreased with time.

We then employed the SEOP method in which nonpolar organic solvents were used. For example, a mixture of oil (hexadecane) and nonpolar organic solvents, such as hexane, octane, and toluene, was prepared at specific ratios ranging from 1 : 6 to 1 : 35. After the mixture at the desired ratio was injected into the membrane, the nonpolar organic solvents gradually evaporated, resulting in the formation of liquid films from the remaining hexadecane. Both the oil and solvent were hydrophobic, and the solvent caused the oil to evaporate. We characterized the thicknesses of the oil films by controlling the ratio of oil to nonpolar organic solvents (Fig. 3a). At a ratio of hexadecane with a corresponding solvent ratio of 6, the film thicknesses for hexane, toluene, and octane were approximately 3.5, 4.5, and 5.5 μm, respectively. As the ratio increased to 35, the film thickness decreased to nearly zero. Interestingly, the rate of decrease in the film thickness was higher for octane and lower for toluene. Moreover, the thickness decreased asymptotically for octane and hexane, remaining stable at a ratio of 35. However, the film disappeared for toluene at a ratio of 30.

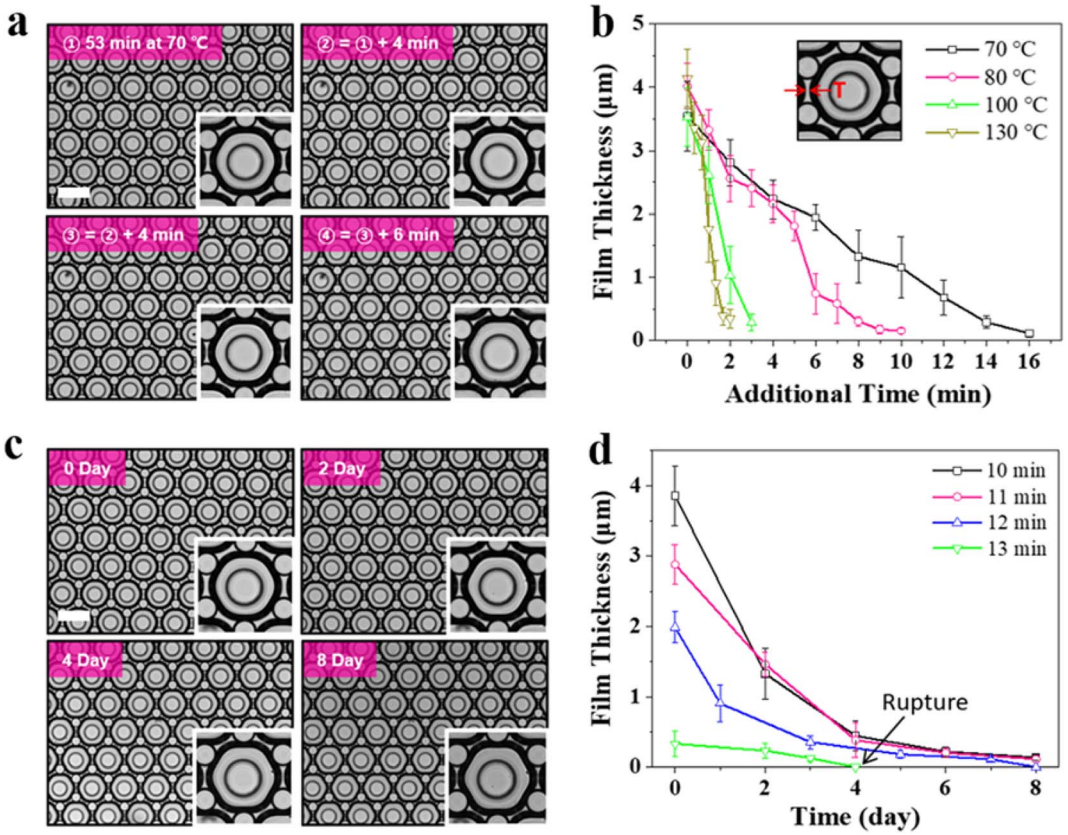

Fig. 2 Characterization of the patterned thickness and durability using heat with hexadecane. (a) Images showing the change in the thickness of oil films at 70 °C. (b) Characterization of changes in the thickness of oil films at four temperatures (70 °C, 80 °C, 100 °C, and 130 °C) applied to the through-hole and post-array membrane. (c) Images of the thickness of liquid films formed at 100 °C overtime. (d) Characterization of the durability of the liquid film at a temperature of 100 °C with four different thicknesses. Error bars represent the standard deviation (SD) of the thickness of the 20 patterned oil films ($N = 20$). Scale bars are 120 μm.

Therefore, for hexadecane–solvent mixtures with low ratios, the film thickness is higher, indicating that the lower the solvent content, the lower the evaporation of oil.

Additionally, the thickness and durability of oil films upon the injection of various ratios of hexadecane and nonpolar organic solvents are illustrated in Fig. 3b–d. As shown in Fig. 3b, when the ratio of hexane to hexadecane was 6, the film thickness was 3.5 μm on day 1 and remained stable up to day 13, maintaining a thickness of approximately 2 μm, whereas, for a ratio of 35, the film was present only for 1 day. When the ratio of hexane was nine times higher than that of hexadecane, the film thickness remained stable for up to 6 days. However, when the ratio of hexane was 25 times higher, the liquid films remained stable for more than 3 days (Fig. 3b). Moreover, the film thickness for the mixture of toluene with hexadecane was maintained at approximately 3 μm for 13 days at a ratio of 6 (Fig. 3c). As depicted in Fig. 3c, the film collapsed on days 9, 10, and 11 for ratios of 9, 12, and 15, respectively; however, the film disappeared in one day at ratios of 20 and 25. Considering the ratio of octane to hexadecane ((Fig. 3d), the film thickness for a ratio of 6 maintained a thickness of 1 μm up to 13; however, the film collapsed in 1 day for ratios of 12–15 and in 2 days for a ratio of 9. Surprisingly, the film thickness decreased drastically from 5.5–2.5 μm on day one at a ratio of 6. Therefore, oil films can be patterned by injecting a mixed solution with varying ratios of hexane, which allows for the formation of oil films with thicknesses ranging from 1–4 μm. Notably, the patterned oil films exhibited long-term stability, with approximately 500 nm thick films persisting for more than 3 days. The oil films patterned with toluene and octane displayed lower durability than those patterned with hexane (Fig. 3c and d). Therefore, when considering the criteria of durability and control over film thickness in the selection of nonpolar organic solvents, hexane has emerged as a suitable choice.

Characterization of the defects of oil films patterned using different configurations of posts and through-holes

Tests were conducted using the SEOP method to assess the presence of defects in the patterned oil films by varying the configurations of through-hole and post arrays in the membrane (Fig. 4). We used hexane, a suitable nonpolar solvent, to pattern the oil film by incorporating a mixture of hexadecane and hexane at a ratio of 1 : 12. The through-hole and post-array configurations used in the experiments were hexagonal (*i.e.*, 6P1H). In the 6P1H, each array consisted of one hole and six posts (Fig. 4d), with a post height of 25 μm, post

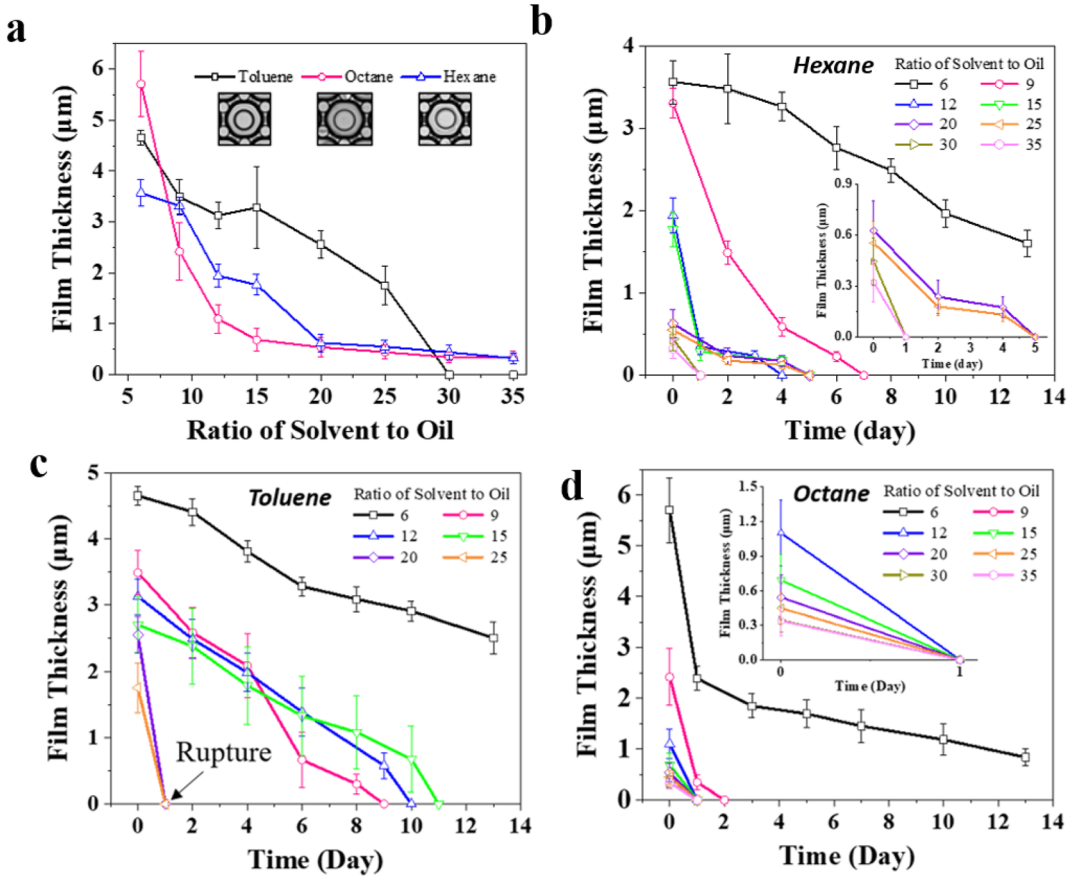

Fig. 3 Characterization of the thickness and durability of patterned oil films using the SEOP method. (a) The thickness of oil films with varying ratios of oil (hexadecane) to nonpolar organic solvents (toluene, octane, and hexane) ranging from 1 : 6 to 1 : 35. (b)–(d) The thickness changes overtime for hexadecane–solvent mixtures: (b) hexane, (c) toluene, and (d) octane. Error bars represent the SD of the thickness of 20 patterned oil films ($N = 20$).

diameter of 15 μm, and hole diameter of 30 μm. This specific structure has been widely employed in various experiments to characterize oil film formation upon solution injection owing to the structural stability of the membrane. As shown in Fig. 4, we attempted to characterize through-hole and post arrays with different shapes and parameters. In addition to hexagonal arrays, it is possible to form oil films even with a rectangular array containing one hole and four posts as the unit of configuration (4P1H) (Fig. 4a). Therefore, the primary parameters that determine the formation of oil films in the through-hole and post arrays are the shape of the arrays, the height of the post (h_p), the diameter of the post (d_p), and the distance between the posts (l).

In the process of fabricating oil films, the foam generated by the air trapped in the hole, which pushed the oil outward, is referred to as an air cell. Fig. 4b illustrates the extent of defects in the formation of oil films when the solution was injected into a device with square arrays under various parameters. The post diameter d_p ranged from 50–80 μm, the distance between the posts l ranged from 40–60 μm, and the height of the post was fixed at 25 μm. When a device with l of 40 μm was used and the solution was injected into the device, the occurrence of defects in the formation of oil films was nearly 0%. However, for a device with $l =$ of 50 μm, the defects were approximately 5% when d_p was set to 80 μm and increased to approximately 30% when d_p was set to 70 μm. Moreover, when d_p is set to 60 and 50 μm, the number of defects increased to approximately 100%. For a device with l set to 60 μm, injecting a solution with the same set of post parameters resulted in defects during the formation of oil films that were approximately 100%. Fig. 4b) shows that, in rectangular arrays, a shorter distance between posts leads to a lower number of defects, whereas a smaller post diameter results in a higher number of defects. In rectangular arrays, each post needs to support four oil films, whereas, in hexagonal arrays, each post only needs to support three oil films. Thus, structures with hexagonal arrays exhibit more stable oil film formation. Further studies with vary parameters of l and d_p supports the observation (refer to Fig. S2 and S3†).

Fig. 4e shows the degree of defect formation in the oil films when the solution was injected into a device with hexagonal arrays under various parameters. d_p ranged from –20–50 μm, l ranged from 30–50 μm, and the height of the post was fixed at 25 μm. When using a device with $l = 30$ μm, the defect rate was 0% when d_p ranged from 30–40 μm; however, the defect rate increased to approximately 60% when d_p was set to 20 μm. For a device with l of 40 μm, the defect rate was 0% when d_p ranged

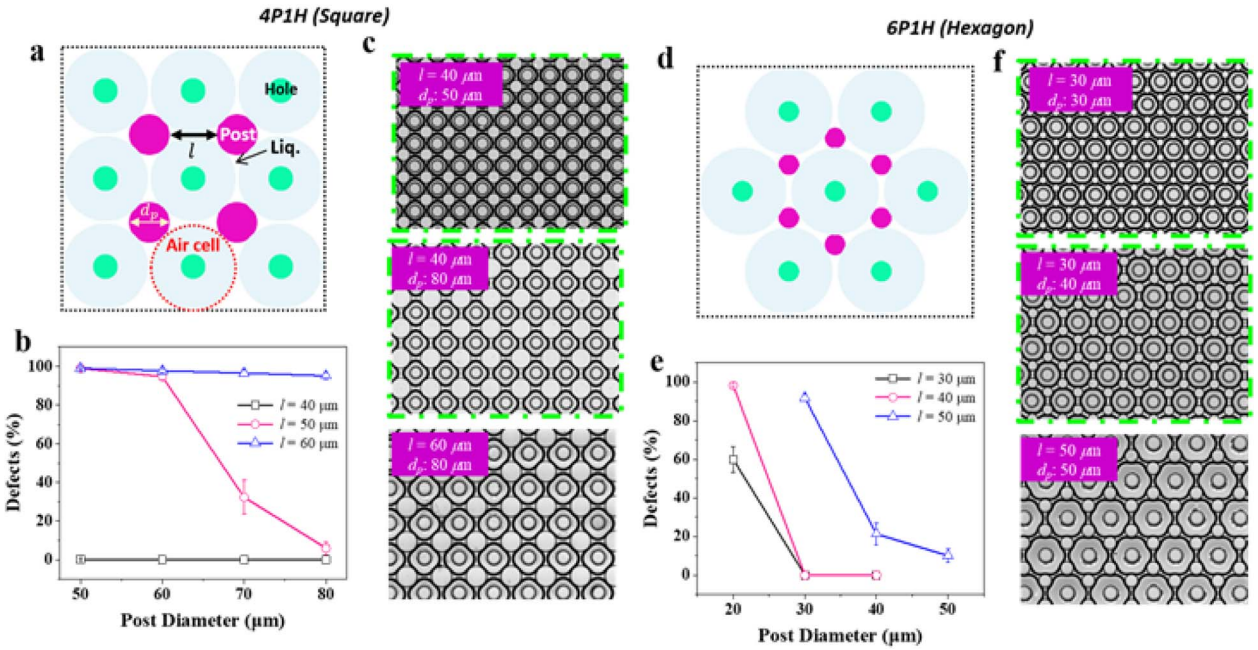

Fig. 4 Characterization of defects in oil films patterned by varying the parameters of through-hole and post arrays. (a) Hole and post arrangement for square arrays. (b) In rectangular arrays, the quantification of defects in oil films with thicknesses ranging from 40–60 μm for l and 50–80 μm for d_p. (c) Images of oil film formation when a 1 : 12 ratio mixture of hexadecane and hexane is injected into square through-hole and post arrays. (d) Hole and post arrangement for hexagonal arrays. (e) In hexagonal arrays, defect quantification of oil films with thicknesses ranging from 30–50 μm for l and 20–50 μm for d_p. (f) Images of oil film formation when a 1 : 12 ratio mixture of hexadecane and hexane is injected into the hexagonal through-hole and post arrays. Error bars represent the SD over the entire patterned area.

from 30–40 μm. However, when d_p was set to 20 μm, the defect rate approached 100%. When a device with $l = 50$ μm was used, the defect rate was 10% when d_p was set to 50 μm, and a defect rate of approximately 20% was observed when d_p was set to 40 μm. Furthermore, when the device with d_p was set to 30 μm, a defect rate of more than 90% was observed. These results suggest that, in hexagonal arrays, a shorter distance between the posts leads to a lower number of defects, whereas a smaller post diameter increases the number of defects. Fig. 4c and f show the images of the oil patterns designed by configuring the arrays of square and hexagonal through-holes and posts with a fixed post height. The diameter of the post (d_p) and the distance between the posts (l) were varied to produce negligible defects in the oil film. For a fixed l, as d_p increased, the diameter of the air–oil interface also increased (Fig. 4c and f (top and bottom)). However, when l increased, the oil–air interfaces were mutually pushed and deformed, eventually attaining a square shape because they were constrained by the solid boundaries. Here, reverse Ostwald ripening was determined by the interval between the pillars.[35]

Application of the SEOP method to photoresists for producing unconventional films/patterns

In our previous work, we demonstrated a water-based material patterning method for forming solidified photoresist films. This approach utilizes a mixture of water and particles, as detailed in the literature.[25] When the mixture is injected into a microfluidic device, the water evaporates, leaving behind aligned particles between the posts due to the strong surface tension of the water. Alternatively, another method involves using photoresists combined with nonpolar organic solvents (Fig. 5). The materials used in the experiment included SU-8 series negative photoresists and AZ series photoresists. The patterning process using SU-8 was similar to the formation of oil films using nonpolar organic solvents. However, when photoresists were used, toluene was the only solvent that satisfied the required conditions. Toluene has a moderate evaporation rate, allowing it to be removed efficiently during post-coating steps without leaving residues that could affect the quality of the photoresist pattern. Additionally, toluene exhibits good solvating properties, effectively dissolving the photoresist material. The solid content of SU-8 photoresists was compared, with SU-8 2005 at 14.3%, SU-8 2002 at 20%, SU-8 2005 at 4%, SU-8 2007 at 52.5%, SU-8 2010 at 58%, and SU-8 2015 at 63.45%. A higher solid content resulted in stronger stickiness, which was advantageous for the formation of solidified films. However, solutions with a solid content higher than that of SU-8 2010 demonstrated problems owing to excessive stickiness, making it difficult to achieve accurate mixing ratios. By contrast, solutions with a lower solid content than that of SU-8 2005 were unsuitable for forming the desired hard films because of their lower viscosity.

In the current experiment, SU-8 2010 was used to form the solidified films. A mixture of SU-8 2010 and toluene in a 1 : 9 ratio was injected into the 6P1H membrane (one hole and six posts formed the same hexagonal unit). After toluene

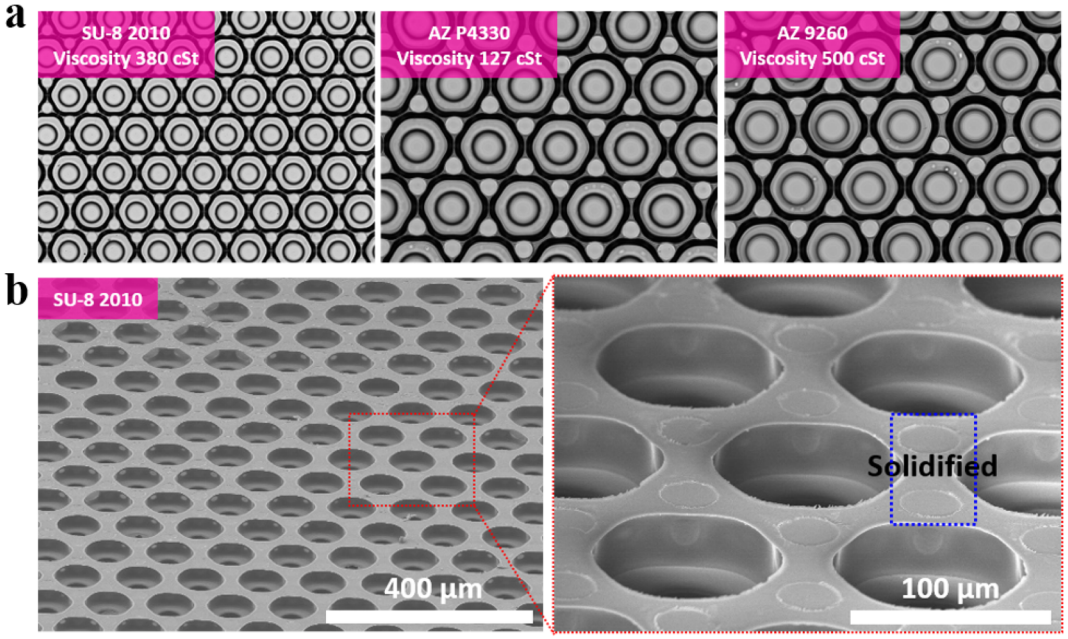

Fig. 5 Patterning organic films with a high aspect ratio and long durability using a mixture of photoresist and toluene. (a) Images obtained by patterning solidified films using negative and positive photoresists. Toluene is completely evaporated by injecting the mixture of photoresist and toluene at a ratio of 1 : 9 into the membrane, and then heating this mixture in an oven at 85 °C for 1 h. Owing to the high viscosity of the photoresist, sticky photoresist films are produced. (b) SEM images of the patterned and solidified SU-8 films (SU-8 2010). The scale bars are 400 μm (left) and 100 μm (right).

evaporated, the trapped air in the hole pushed out the photoresists, resulting in the formation of liquid films with air–photoresist interfaces. To ensure complete evaporation of the residual toluene and further hardening of the remaining photoresists, the membrane was heated in an oven at 85 °C for 1 h. Patterning was also performed using the AZ series photoresists, following the same process as that used for the SU-8 series. The AZ series photoresists were mixed with toluene at a ratio of 1 : 9 and then injected into the 6P1H membrane. The toluene evaporated, and the air trapped in the hole pushed out the AZ photoresists, forming liquid films with air–photoresist interfaces. The membrane was then heated in an oven at 85 °C for 1 h to allow for the complete evaporation of residual toluene and hardening of the photoresists. Viscosity plays a significant role in the formation of solidified films when using the AZ series photoresists. Among the AZ photoresists used, AZ P4330 and AZ 9260 with viscosities of 127 cSt and 500 cSt, respectively, exhibited the most stable patterning, as shown in Fig. 5a. The high viscosity of these photoresists allowed the films to withstand contact with air at the air–photoresist interfaces without bursting or collapsing. Once formed, the solidified films remained in their original state even after several days. Fig. 5a shows the images obtained by patterning solidified films using negative photoresist SU-8 2010 and positive photoresist AZ P4330 and Az 9260. The liquid film thickness using AZ P4330 was 3–5 μm, which increased to 5–20 μm for AZ 9260 owing to the increase in viscosity. Fig. 5b shows the SEM images of the patterned (left) and solidified (right) SU-8 films (SU-8 2010), depicting the high aspect ratio grids. Notably, these photoresist films/patterns are facile and low-cost compared to conventional standard photolithography and/or soft lithography.

Bending test of oil films patterned on a flexible substrate and their future applications

The patterning of liquid films was performed on a flat substrate because the substrate had little effect on whether it was flat or curved (Fig. 6). The oil films patterned on flat substrates remained intact even when bent to a radius of curvature of 3 mm. Fig. 6a shows an optical image of the transparent and flexible device on which the oil film was printed. We examined the stability of an oil film printed on a curved substrate with curvatures of 0.14 mm^{-1} and 0.33 mm^{-1}, as shown in Fig. 6a and b, respectively. The oil film was almost unaffected even when the bending stress was applied by repeatedly bending it for 100 cycles up to a curvature of 0.33 mm^{-1}. At a low curvature (0.14 mm^{-1}, as shown in Fig. 6b), thick and narrow grids were printed compared with those at a high curvature (0.33 mm^{-1}, as shown in Fig. 6c), in which a thin and wide-grid oil film was printed.

Liquid films have significantly higher aspect ratios than solid grids and demonstrate high flexibility and flexural strength. Consequently, if the self-assembly of a conductive material is also performed, this technique could be employed as a novel concept for electrodes with improved conductivity. Furthermore, we successfully patterned solid organic films with high aspect ratios using the photoresist and toluene. To address the limitation of patterning only after the complete evaporation of the liquid, we successfully fabricated liquid films with long-

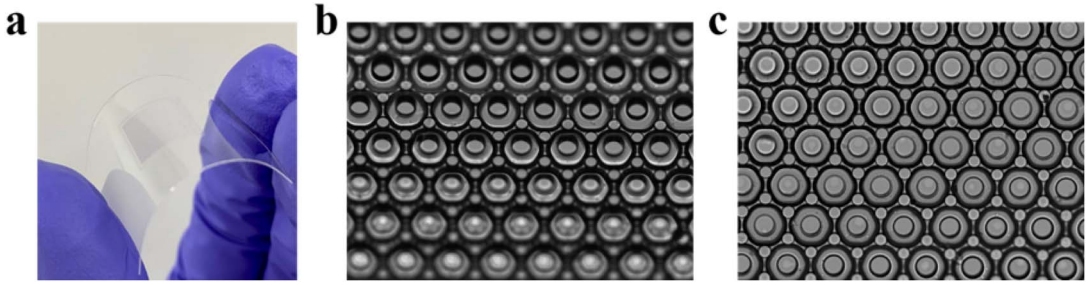

Fig. 6 Oil films patterned on curved and flexible substrates are subjected to repeated bent tests to showcase their flexibility and durability. (a) Photograph of a transparent and flexible device with patterned oil films on its surface. (b) Image showing the oil films while being bent with a curvature of 0.14 mm^{-1}. (c) Image showing the oil films in a flat state after undergoing 100 cycles of repeated bending tests with a curvature of 0.33 mm^{-1}.

term stability using oils and nonpolar organic solvents. These liquid films have significant potential for liquid electrode patterning, primarily because of their high aspect ratios and durability. When conductive materials are applied to these liquid films, they are expected to exhibit enhanced electrical properties compared with solid conductive grids. Moreover, the technique used to fabricate liquid films can be repeatedly used and implemented on flexible substrates in a simple and low-cost manner, offering a novel fabrication strategy with high potential for flexible electronics and next-generation wearable systems. By transitioning from a water-containing dispersion to oil to fabricate liquid films, we successfully overcame the limitations associated with patterning electrodes. This breakthrough opens up new possibilities for expanding the range of next-generation electronic applications. Furthermore, we present additional evidence that harnessing the flow behavior is a versatile and feasible strategy for patterning various functional materials, ranging from inorganic, organic, and hybrid to biological categories, on diverse substrates. This demonstrates the great potential for practical applications in various fields, including microelectronics, optics, filtration and separation, biomedical engineering, and nanotechnology.

It is noteworthy to discuss the characteristics of DHOP and SEOP. DHOP primarily uses organic oil and heat sources, whereas SEOP employs a mixture of oil and a volatile organic solvent that dissolves the oil at room temperature. To create organic oil patterns, both methods introduce either pure oil or an oil–solvent mixture into the microfluidic template or device. However, DHOP applies heat to evaporate the oil at high temperatures, while SEOP allows only the volatile solvent to evaporate, forming the thin oil patterns as designed. As a result, controlling the boiling points of both the oil and the solvent is essential to creating a variety of oil patterns. It is noted that SEOP relies solely on the evaporation of the volatile solvent at room temperature, ensuring that the oil itself does not evaporate during the patterning process. In summary, there are several ways to compare the advantages and disadvantages of the two methods. From the perspective of oil pattern thickness, DHOP is more suitable for organic oils with low boiling points, while SEOP works best with oils that are highly soluble in the chosen solvents. Stability and durability are another factors to consider; oil patterns created by DHOP tend to last longer due to the intrinsic properties of the oils used. However, SEOP patterns also demonstrate sufficient stability and durability for a variety of applications. The SEOP method was specifically developed for target materials, including oils that dissolve well in volatile solvents and are sensitive to evaporation due to their low boiling points. As demonstrated, SEOP can produce film patterns without the need for high temperatures, highlighting the process simplicity and fabrication convenience. Without a volatile solvent, producing the same pattern at room temperature could take several weeks. Consequently, both DHOP and SEOP offer unique characteristics and play important roles in generating thin films from a wide range of materials in an unconventional manner.

Conclusions

In this study, we demonstrated a liquid patterning method on transparent, flexible, and curved substrates utilizing oil and nonpolar organic solvents. Patterning was achieved using the TGF method, which involves the use of a thin membrane film integrated with through-hole and post arrays. We employed the DHOP and SEOP methods using hexadecane as the oil component and toluene, octane, and hexane as solvents. To ensure the long-term stability of the liquid films, oil was injected at low evaporation rates, whereas nonpolar organic solvents were used to induce slight evaporation. The durability of the liquid films developed in this study was demonstrated by the ability to control the thickness of the films by adjusting the ratio of organic solvents, thus maintaining a thickness of less than 1 μm for up to 1 day. By considering the criteria of durability and control over film thickness, hexane has emerged as a suitable choice among nonpolar organic solvents for future applications. Furthermore, liquid films exhibit significantly higher aspect ratios than solid grids and demonstrate remarkable flexibility and flexural strength. Consequently, when combined with the self-assembly of conductive materials, they can serve as innovative electrodes with enhanced conductivity. In addition, this study revealed that the stability of the liquid film pattern using hexadecane and hexane was enhanced when the through-hole and post arrays within the membrane have hexagonal configurations. We observed that shorter distances between the posts resulted in lower defect percentages, whereas reducing

the diameter of the posts led to higher defect percentages. Finally, we utilized a mixture of toluene and an organic photoresist to fabricate unconventional solid organic films that could not be produced using conventional standard photolithography techniques. Owing to their higher aspect ratio and increased durability compared with liquid films, organic films show significant potential for future electrode development using conductive organic semiconductor materials. Hence, we believe that our study offers a novel fabrication strategy for the development of high flexural strength, durable, and water-free thin liquid films, thereby presenting the potential to expand the range of next-generation electronic applications.

Data availability

The data that support the findings of this study are available from the corresponding author upon reasonable request.

Author contributions

This study was conceived by T. K., and the development of the microfluidic one-step printing method enabling oil patterning was performed by Y. C. and J. B. Y. C. conducted all the experiments with assistance from J. B. All authors participated in discussions on the experimental results. The manuscript was written by T. K. with input and approval from all authors.

Conflicts of interest

The authors declare no competing financial interests.

Acknowledgements

This work was supported by a grant from the Institute for Information and Communications Technology Promotion (IITP) funded by the Korean government (MSIT) (No. 2022-0-00062) and a grant from the National Research Foundation of Korea (NRF) funded by the Korean government (MSIT) (No. 2020R1A2C3003344).

References

1 D. E. Kataoka and S. M. Troian, *Nature*, 1999, **402**, 794–797.
2 P. Ferraro, S. Coppola, S. Grilli, M. Paturzo and V. Vespini, *Nat. Nanotechnol.*, 2010, **5**, 429–435.
3 Z. Huang, M. Su, Q. Yang, Z. Li, S. Chen, Y. Li, X. Zhou, F. Li and Y. Song, *Nat. Commun.*, 2017, **8**, 14110.
4 S. Witomska, T. Leydecker, A. Ciesielski and P. Samorì, *Adv. Funct. Mater.*, 2019, **29**, 1901126.
5 B. Ma, C. Xu, J. Chi, J. Chen, C. Zhao and H. Liu, *Adv. Funct. Mater.*, 2019, **29**, 1901370.
6 R. Zhang, S. A. Redford, P. V. Ruijgrok, N. Kumar, A. Mozaffari, S. Zemsky, A. R. Dinner, V. Vitelli, Z. Bryant, M. L. Gardel, *et al.*, *Nat. Mater.*, 2021, **20**, 875–882.
7 K. S. Park, J. Baek, Y. Park, L. Lee, Y.-E. K. Lee, Y. Kang and M. M. Sung, *Adv. Mater.*, 2016, **28**, 2874–2880.
8 K. S. Park, K. S. Lee, J. Baek, L. Lee, B. H. Son, Y.-E. Koo Lee, Y. H. Ahn, W. I. Park, Y. Kang and M. M. Sung, *Angew. Chem.*, 2016, **128**, 10429–10433.
9 J. Bae, K. Lee, S. Seo, J. G. Park, Q. Zhou and T. Kim, *Nat. Commun.*, 2019, **10**, 3209.
10 S. Lone, J. M. Zhang, I. U. Vakarelski, E. Q. Li and S. T. Thoroddsen, *Langmuir*, 2017, **33**, 2861–2871.
11 D. Yamamoto, C. Nakajima, A. Shioi, M. P. Krafft and K. Yoshikawa, *Nat. Commun.*, 2015, **6**, 7189.
12 L. Keiser, H. Bense, P. Colinet, J. Bico and E. Reyssat, *Phys. Rev. Lett.*, 2017, **118**, 074504.
13 C. Minas, D. Carnelli, E. Tervoort and A. R. Studart, *Adv. Mater.*, 2016, **28**, 9993–9999.
14 Z. Li, Z. Huang, F. Li, M. Su, H. Li, Z. Zhang, Y. Wang and Y. Song, *ACS Appl. Mater. Interfaces*, 2019, **11**, 17960–17967.
15 P. Zhu, T. Kong, X. Tang and L. Wang, *Nat. Commun.*, 2017, **8**, 15823.
16 X. Wan, X. Xu, X. Liu, L. Jia, X. He and S. Wang, *Adv. Mater.*, 2021, **33**, 2008557.
17 Z. Wang, Y. Xu, N. Khan, C. Zhu and Y. Gao, *J. Mol. Liq.*, 2023, **373**, 121194.
18 W. Deng, X. Zhang, L. Huang, X. Xu, L. Wang, J. Wang, Q. Shang, S.-T. Lee and J. Jie, *Adv. Mater.*, 2016, **28**, 2201–2208.
19 S. Li, Y. T. Chun, S. Zhao, H. Ahn, D. Ahn, J. I. Sohn, Y. Xu, P. Shrestha, M. Pivnenko and D. Chu, *Nat. Commun.*, 2018, **9**, 393.
20 J. Feng, X. Jiang, X. Yan, Y. Wu, B. Su, H. Fu, J. Yao and L. Jiang, *Adv. Mater.*, 2017, **29**, 1603652.
21 J. K. Hwang, S. Cho, J. M. Dang, E. B. Kwak, K. Song, J. Moon and M. M. Sung, *Nat. Nanotechnol.*, 2010, **5**, 742–748.
22 J. H. Maurer, L. González-García, B. Reiser, I. Kanelidis and T. Kraus, *Nano Lett.*, 2016, **16**, 2921–2925.
23 J. Han, J. Yang, W. Gao and H. Bai, *Adv. Funct. Mater.*, 2021, **31**, 2010155.
24 V. Sharma, A. Koivikko, K. Yiannacou, K. Lahtonen and V. Sariola, *npj Flex. Electron.*, 2020, **4**, 27.
25 Y. Chae, J. Bae, K. Lim and T. Kim, *RSC Adv.*, 2022, **12**, 27846–27854.
26 R. Geczy, D. Sticker, N. Bovet, U. O. Häfeli and J. P. Kutter, *Lab Chip*, 2019, **19**, 798–806.
27 J. Bae, Y. Chae, J. G. Park, R. Wu, J. Ju and T. Kim, *ACS Appl. Mater. Interfaces*, 2021, **13**, 19168–19175.
28 J. Li, Q. H. Qin, A. Shah, R. H. Ras, X. Tian and V. Jokinen, *Sci. Adv.*, 2016, **2**, e1600148.
29 D. Tahk, S.-M. Paik, J. Lim, S. Bang, S. Oh, H. Ryu and N. L. Jeon, *Lab Chip*, 2017, **17**, 1817–1825.
30 J. Bae, J. Lee, Q. Zhou and T. Kim, *Adv. Mater.*, 2019, **31**, 1804953.
31 D. Sticker, M. Rothbauer, S. Lechner, M.-T. Hehenberger and P. Ertl, *Lab Chip*, 2015, **15**, 4542–4554.
32 J. H. Yao, K. Elder, H. Guo and M. Grant, *Phys. Rev. B: Condens. Matter Mater. Phys.*, 1993, **47**, 14110.
33 R. I. Saye and J. A. Sethian, *Science*, 2013, **340**, 720–724.
34 S. I. Karakashev and E. D. Manev, *Adv. Colloid Interface Sci.*, 2015, **222**, 398–412.
35 R. Lemlich, *Ind. Eng. Chem. Fundam.*, 1978, **17**, 89–93.